Author(s): Laitinen, Mikko; Rossi, Mikko; Julin, Jaakko; Sajavaara, Timo

Title: Time-of-flight - Energy spectrometer for elemental depth profiling - Jyväskylä design

Year: 2014

Version:

Time-of-flight – energy spectrometer
for elemental depth profiling - Jyväskylä design

Mikko Laitinen, Mikko Rossi, Jaakko Julin, Timo Sajavaara

Dept. of Physics, P.O.Box 35, 40014 University of Jyväskylä, Finland

Corresponding author: Mikko Laitinen
Telephone : +358 400 994836
Fax: +358 14 617411
E-mail: mikko.i.laitinen@jyu.fi

Abstract:
A new time-of-flight elastic recoil detection spectrometer has been built, and initially the main effort was focused in getting good timing resolution and high detection efficiency for light elements. With the ready system, a 154 ps timing resolution was recorded for scattered 4.8 MeV ^{4}He^{2+} ions. The hydrogen detection efficiency was from 80 to 20 % for energies from 100 keV to 1 MeV, respectively, and this was achieved by having an additional atomic layer deposited Al_2O_3 coating on the first timing detector's carbon foil. The data acquisition system utilizes an FPGA-card to time-stamp every time-of-flight and energy event with 25 ns resolution. The different origins of the background events in coincident time-of-flight–energy histograms have been studied and explained. The built system has proved to be able to routinely depth profile films thinner than 10 nm.

1 Introduction

Time-of-Flight Elastic Recoil Detection Analysis (ToF-ERDA), originally developed in the 1980's [1--3], is used to depth profile elemental compositions most commonly from thin films. In this method, an ion beam in the energy range of few MeVs to tens of MeVs is used to bombard the sample and to recoil the sample atoms towards the ToF-ERD detector telescope. Time-of-flight and energy (ToF-E) recorded in coincidence allow to differentiate masses and to depth profile all sample elements, including hydrogen. This powerful technique has the advantage that it provides quantitative results by means of the known kinematics, cross sections and stopping forces obtained from e.g. ZBL formulation [4] or from the SRIM [5] without the need to use reference samples.

Due to its linear behavior and better resolution [1,6], the energy calculated from the ToF signal is generally used for the actual depth profiling and E-detector data only for the separation of different masses. The mass separation depends on the TOF and energy detector resolutions and the incoming particle energy. The Jyväskylä setup was originally designed to use a standard silicon charged particle energy detector although these detectors are known to have poor energy resolution for low energy heavy mass particles [1,7]. One can, however, achieve good energy resolution also for the low energy heavy particles by using a gas ionization detector with thin Si_3N_4 windows [8].

More recent ToF-ERDA tools, comprising two carbon foil time pick-up detectors [9] (timing gates for short) and an energy detector, have been built for example in Zurich [10], Leuven/IMEC [11] and Zagreb [12]. These systems report ToF-distances of 100 cm, 57 cm and 52 cm, respectively. First one utilizes a gas ionization detector as an energy detector and at least the first carbon foil is made of diamond like carbon (DLC), and the DLC start foil of the Zagreb system has LiF coating to enhance the secondary electron emission from the foil. In Zurich a separate detector is used to detect hydrogen but in the other two setups mentioned above, up to 60 % detection efficiencies for hydrogen are reported. Intrinsic timing resolutions of 400 ps and 170 ps are reported for the Zurich [13] and Zagreb systems while measured timing resolution of 550 ps is reported for the Leuven/IMEC. Solid angles of the comparing systems are 0.26 msr (~0.2 msr with Si_3N_4 window supports) [10], 0.44 msr [11] and 0.11 msr [12], respectively. Data acquisition of all of these systems, although not mentioned in the listed references, has been traditional analogue coincidence-type list-mode event data.

The three setups mentioned above have the same goal, elemental depth profiling of thin films, but the designs could be seen to have bit different philosophies. These could be categorized as aiming for: high heavy mass resolution and hydrogen detection with additional detector outside the telescope (Zurich), large solid angle to minimize beam damage for sensitive samples (Leuven/IMEC) and smaller solid angle with good timing resolution to achieve good depth resolution accompanied with the enhanced hydrogen detection efficiency (Zagreb). Similar design features always need to be considered when building a new ToF-ERDA tool and trade-offs in the performance are sometimes necessary.

82 In this work we have designed and taken into use a new ToF-ERD setup in Jyväskylä.
83 The setup has hydrogen detection efficiency of 40-80 % for relevant energy region (< 500
84 keV), surface depth resolution reaching 1 nm for thin film samples and low background
85 on measured histograms. These figures of merit were made possible by focusing on
86 detection efficiency, ToF resolution and to the development of the data acquisition (DAQ)
87 system. Here we report the system and its detailed performance figures.
88
89

90 **2 Experimental setup**

91

92 The ToF-E spectrometer has 6-axis goniometer for sample adjustment and a scattering
93 chamber with a load lock. It was built to the +15 degree beamline after the switching
94 magnet of the 1.7 MV Pelletron accelerator in Jyväskylä. The ToF-E telescope scattering
95 angle is 41.3(2) degrees and the ToF distance is 623(1) mm. A schematic CAD-drawing
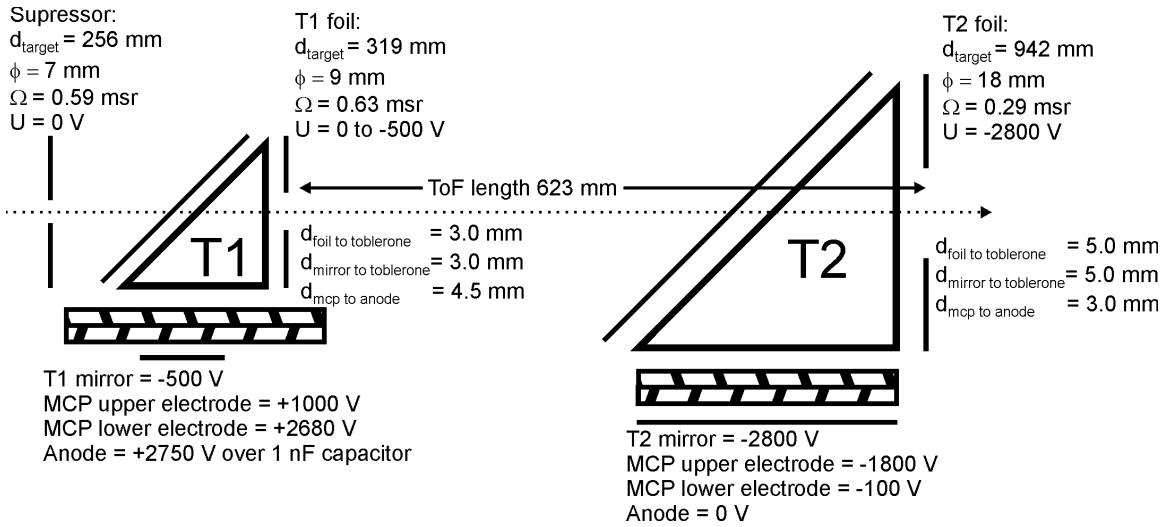96 of the setup is shown in the Fig. 1.
97
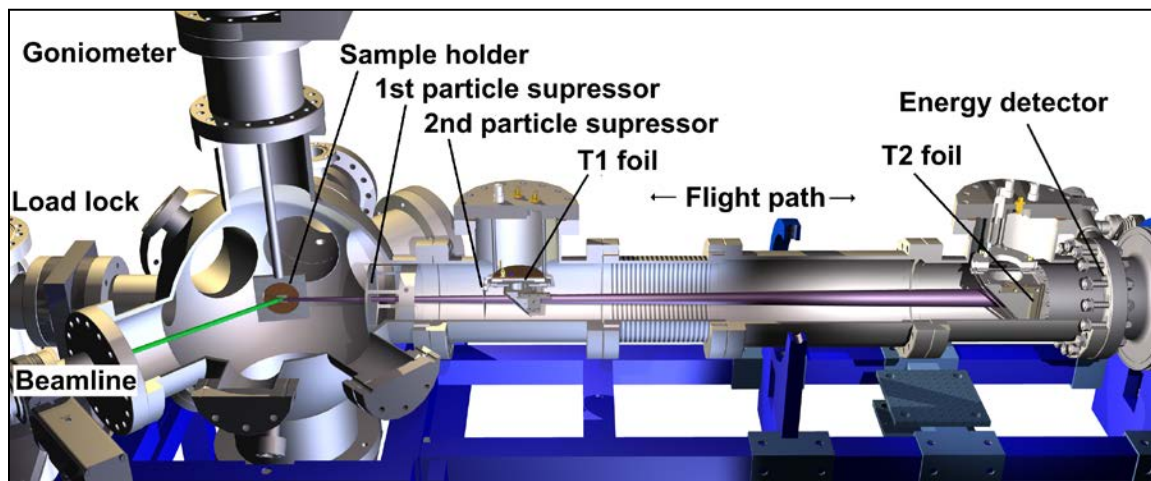
98

99 *Figure 1. Schematic view of the ToF-ERD spectrometer. Telescope angle is 41.3 degrees*
100 *relative to the ion beam. Energy detector in the image is a pre-production version of the*
101 *upcoming gas ionization detector, but current results are measured with the plain silicon*
102 *charged particle energy detector located similarly just after the T2 foil.*

103 **2.1 Detectors**

104

105 Originally the voltages of the both timing gates were identical (similar to current T2) but
106 the operation voltages of the first timing gate were afterwards changed in order to
107 minimize the possible tandem effect [14]. Now the carbon foil of the T1 is grounded and
108 the anode voltage is raised to a potential of +2800 V (See Figs. 2 and 3). The second
109 improvement was the addition of about 1 nm thick atomic layer deposited (ALD) Al_2O_3
110 film to the first carbon foil in order to increase the secondary electron emission and
111 thereafter also the detection efficiency.
112

Supressor:
d_{target} = 256 mm
ϕ = 7 mm
Ω = 0.59 msr
U = 0 V

T1 foil:
d_{target} = 319 mm
ϕ = 9 mm
Ω = 0.63 msr
U = 0 to -500 V

T2 foil:
d_{target} = 942 mm
ϕ = 18 mm
Ω = 0.29 msr
U = -2800 V

ToF length 623 mm

T1

T2

$d_{foil\ to\ toblerone}$ = 3.0 mm
$d_{mirror\ to\ toblerone}$ = 3.0 mm
$d_{mcp\ to\ anode}$ = 4.5 mm

$d_{foil\ to\ toblerone}$ = 5.0 mm
$d_{mirror\ to\ toblerone}$ = 5.0 mm
$d_{mcp\ to\ anode}$ = 3.0 mm

T1 mirror = -500 V
MCP upper electrode = +1000 V
MCP lower electrode = +2680 V
Anode = +2750 V over 1 nF capacitor

T2 mirror = -2800 V
MCP upper electrode = -1800 V
MCP lower electrode = -100 V
Anode = 0 V

113

114 *Figure 2. ToF-telescope dimensions, measures and nominal operation voltages.*

115

116 The microchannel plates (MCP), provided by TECTRA [15], and used in both of the
117 timing gates, have an outer diameter of 50 mm, maximum active diameter of >40 mm, 12
118 μm pore size and 1:40 d/L ratio. Both timing gates have about the same potential
119 differences: MCPs are operated at 1700 V over the Chevron stack, MCP to anode
120 potential is about +100 V, and the MCP surface electrode potential is about +1 kV higher
121 than the carbon foil potential, see Figs. 2 and 3. In our MCP configuration there is no
122 potential difference between the MCP plates but the two microchannel plates have 0.3
123 mm thick spacer ring between them. The ~1 kV potential which is used to accelerate the
124 electrons from the foil to the MCP gives close to optimum electron detection energy for
125 the MCPs [16--18]. The measured saturation region in the MCP efficiency, however,
126 seems to start already at 200 eV with nominal MCP voltages, but for example in the case
127 of T1, the foil and mirror is kept at -500 V to minimize the number of free electrons
128 flying towards the timing gate and the MCP.
129
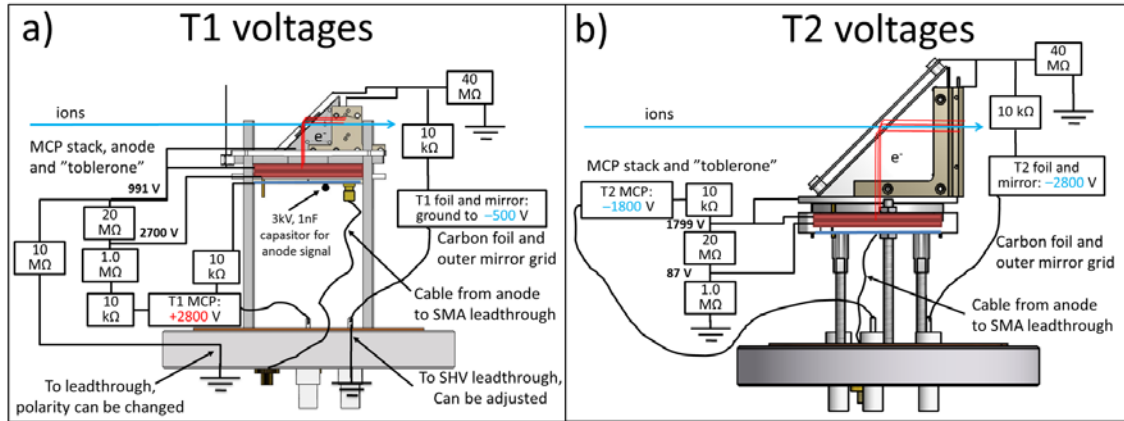
Figure 3. Resistor/voltage configuration of the timing gates. For T1 the foil can be grounded, but the foil and mirror are normally set to -500 V potential to reduce the number of unwanted events due to low energy electrons. The usage of two HV power supplies in both timing gates enables flexible tuning of the voltages.

The thickness of the carbon foils (mainly supplied by [19]) is currently 3 $\mu g/cm^2$ (+ 1 nm Al_2O_3) for the first timing detector (T1) and 7 $\mu g/cm^2$ for the second (T2). The foil diameter is 9 mm and 18 mm for T1 and T2, respectively, giving the current system a solid angle of 0.29 msr (see Fig. 2). This can, however, be maximized to >1.4 msr by using the whole active area of the T2 MCP once the kinematic correction currently under development is taken into use. Electron mirror- and toblerone-part grids are made from 20 and 25 μm diameter Au plated tungsten wire [20], point welded with 1 mm spacing. With the point welded thin wires, the optical transmission of the whole ToF-telescope, with six grids, is 86 % (thus the active solid angle is ~0.25 msr).

The energy-detector in this study is a standard 450 mm^2 ion implanted charged particle detector, [21]) right after the T2 carbon foil. Gas ionization chamber for the E-detector replacement is under a testing period. Especially for the measurements with low energy incident ions the gas ionization detector offers superior energy resolution [7,8] and comes with a native position sensitivity [22].

2.2 Analogue electronics and DAQ

Signals from the two timing gates are fed to the 10x preamplifier (Phillips Scientific 776) and further to the Ortec 935 constant fraction discriminator (CFD). Logic pulses from the CFD are then processed in FAST 7072T dual TDC/ADC so that T1 gives a start pulse and T2 a stop pulse. Energy signal from the E-detector is fed through the Ortec 142 preamplifier to the Ortec 571 shaping amplifier with 1 μs shaping time. After the shaping amplifier the energy pulse height is analyzed by the same FAST TDC/ADC -unit having a fixed 500 ns conversion time.

ToF and E events are retrieved from the TDC/ADC -unit and are time stamped by the National Instruments PXI-7811R-FPGA module [23]. The clock frequency of the FPGA

164 is 40 MHz providing 25 ns time stamp resolution. DAQ control software programmed
165 with LabVIEW is used for the online monitoring of the measurement. Control software
166 also enables, for example, online count rate monitoring, quick check-up of detector
167 efficiencies and different ROI selections for the collected statistics control during the
168 measurements.
169
170 **3 Results**
171
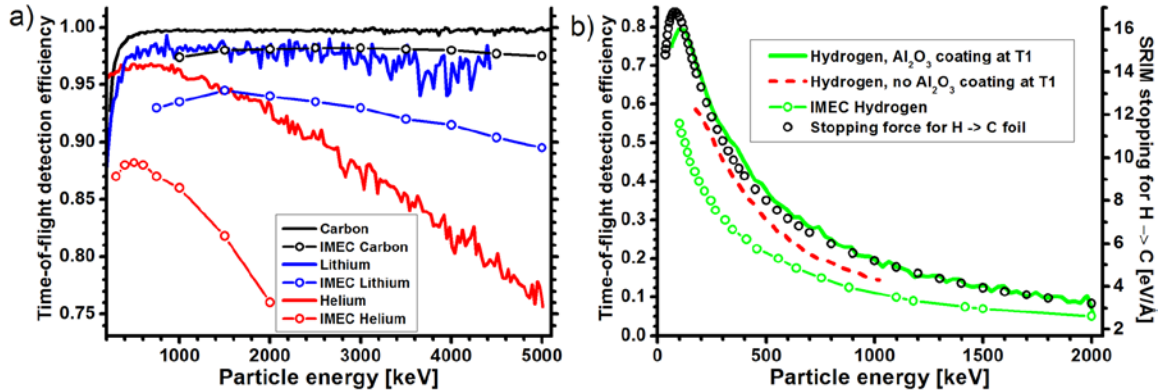172 **3.1 Detection efficiency**
173
174 The detection efficiency of the silicon detector can be expected to be 100 % for the ions
175 hitting the detector in the energy range typically used in the ion beam analysis, but the
176 detection efficiency of the timing unit consisting of two carbon foil time pick-up
177 detectors can be considerably lower. To measure the detection efficiency of the two
178 timing units, we have compared the events in the silicon detector to the events from the
179 ToF detector and expected the efficiency of the Si detector to be 100 %. For a single
180 carbon foil time pick-up detector, the detection efficiency is mainly dependent on the
181 number of emitted secondary electrons from the foil and their multiplication in the MCP.
182 The electron emission probability is material dependent and for a single foil it follows the
183 electronic stopping force of the foil for particular ion [24--26]. Due to the small number
184 of emitted secondary electrons, the detection efficiency for the light elements is often
185 below 100 %. Full detection efficiency can be reached for heavier elements (see for
186 example Fig. 4) if no pinholes exist in the foils. The foil thickness also affects the
187 secondary electron emission intensity if the carbon foil thickness is below 10 μg cm^{-2}
188 [27].
189
190 As the quantitative detection of light impurities, especially hydrogen, is one of the key
191 characteristics of the ToF-ERD method, we have tried to enhance the hydrogen detection
192 efficiency. A thin LiF-coating on the carbon foil has earlier been used by others to
193 increase the number of secondary electrons [12,28]. For the same purpose, we deposited
194 1 nm Al_2O_3 layer by ALD on the electron emission side of the T1 carbon foil. The ALD
195 film was deposited using TMA (trimethylaluminum) and H_2O as precursors [29] at 100
196 ºC. For T2 carbon foil, despite several trials, we did not succeed to mount the much larger
197 carbon foil with the Al_2O_3 layer on it. The measured increased detection efficiencies for
198 different light elements are shown in the Fig. 4. The relative detection efficiency increase
199 is greater for higher energies, being 56% $\rightarrow$ 65% at 200 keV and 14.5% $\rightarrow$ 19.5% at 1
200 MeV. From the Ref. [27], however, it is worth to notice that a native impurity layer on
201 the foil surface, compared to sputter cleaned carbon foil, also enhances the electron
202 emission up to 100 % for the smallest electron emission energies (< 10 eV). This layer
203 can originate, for example from the lift-off process of the carbon foil from water to the
204 foil holder. For the reference, in the Fig. 4, the corresponding detection efficiencies for
205 the ToF-ERD spectrometer at IMEC [11] are presented.
206

Figure 4. Detection efficiency for different ions as a function of energy. In a) the detection efficiencies for He, Li and C are shown together with efficiencies of another ToF-ERD system [11]. For carbon our detection efficiency is better than 99.5 % and those events missing from 100 % are a result of events with a wrong time-of-flight (count rate effect) and not from the pinholes in the foil. In b) the detection efficiency curve for the hydrogen is shown together with the SRIM stopping data for hydrogen. Even though only the first timing gate has the Al_2O_3 coating, the hydrogen detection efficiency is clearly better for energies below 1 MeV.

3.2 Timing resolution

The second important figure of merit of the ToF-ERD spectrometer is the timing resolution. Our large diameter MCP detectors were originally equipped with 50 mm diameter plate shaped anodes made of stainless steel. The anodes were located about 1.0 mm from the MCP electrode and this original configuration gave about 2 ns signal rise time (10% $\rightarrow$ 90%). New 19 mm and 43 mm diameter anodes were made from standard printed circuit board for T1 and T2, respectively. By changing the anode material, contact method to SMA connector, reducing the anode active size and by increasing the distance from the MCP electrode to the anode to 2.5 mm, the rise times dropped to about 1 ns for both T1 and T2 signals (see Fig. 5).

229
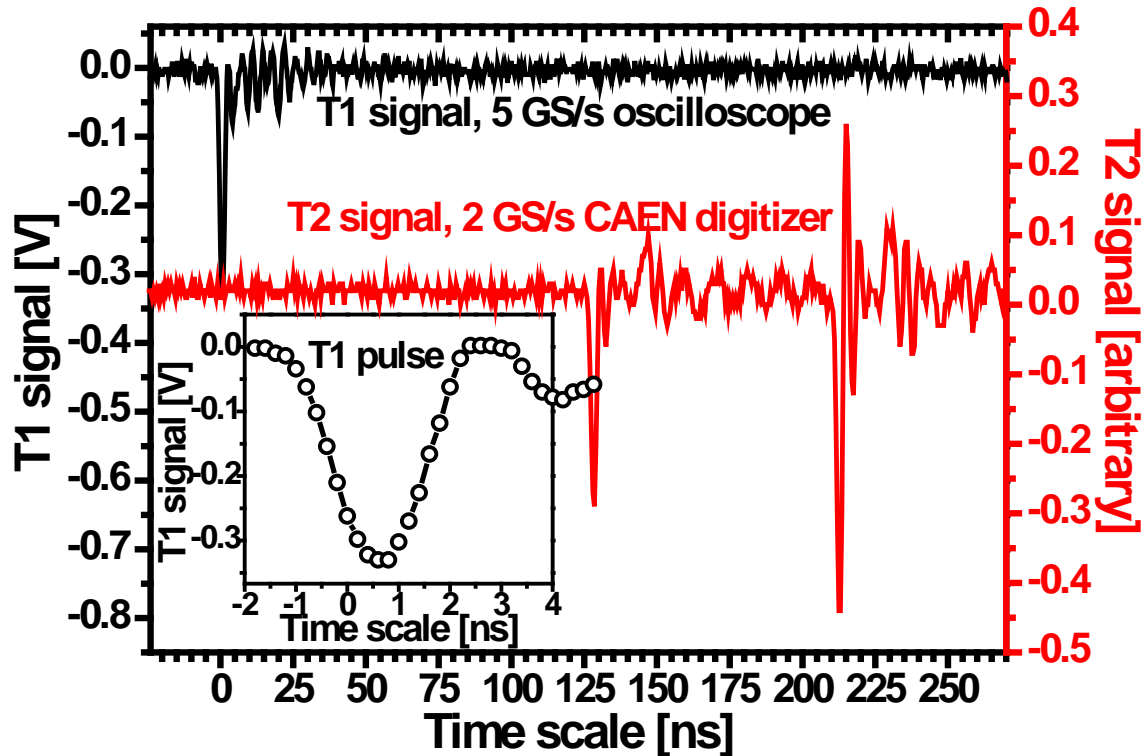
Figure 5. Preamplified MCP signals from T1 and T2 detectors representing the start and stop events, respectively. The shown signals originate from different events but represent general average-signals from the timing gates. T1 signal has generally been somewhat weaker, but having also less oscillations, whereas T2 signals show strong constant oscillation or 'ringing' after the main pulse. For T2 there are actually two different events and possibly a wrong ToF-event as a result. The insert shows a magnification of the T1 main pulse.

With Ortec 935 CFD we have recorded a 154 ps timing resolution (peak FWHM) for an incident 4.8 MeV ^{4}He^{2+} beam which was scattered from a thin Au film towards the detector telescope (see insert in Fig. 6). The energy resolutions calculated from the timing signals for the scattered H, He, C and Cl ions for a wide energy range are shown in a Fig. 6. Results in the Fig. 6 include incident ion energy spread, kinematic spread and the non-uniformity of the electron beam evaporated Au scatterer film. For the 250 keV He the resolution, when converted to energy, is close to 5 keV from which about 2 keV could be due to the 10 % T1 carbon foil thickness variation and energy straggling in it. Also, as seen from Fig. 6, the relative TOF energy resolution becomes worse for all ions at lower energies. Although relative contribution of straggling to the energy resolution does increase at lower energies, it does not fully explain this effect which we believe to originate mainly from the thickness non-uniformity of the Au scatterer film and the T1 foil. The resolution degradation at smaller energies could possibly be reduced by using even thinner DLC-foils (diamond like carbon) [8,30,31] for secondary electron emission. Very thin DLC-foils, however, need a supporting grid [8], normally suffer from pinholes and while being so thin, can also have poorer hydrogen detection efficiency [27].

254
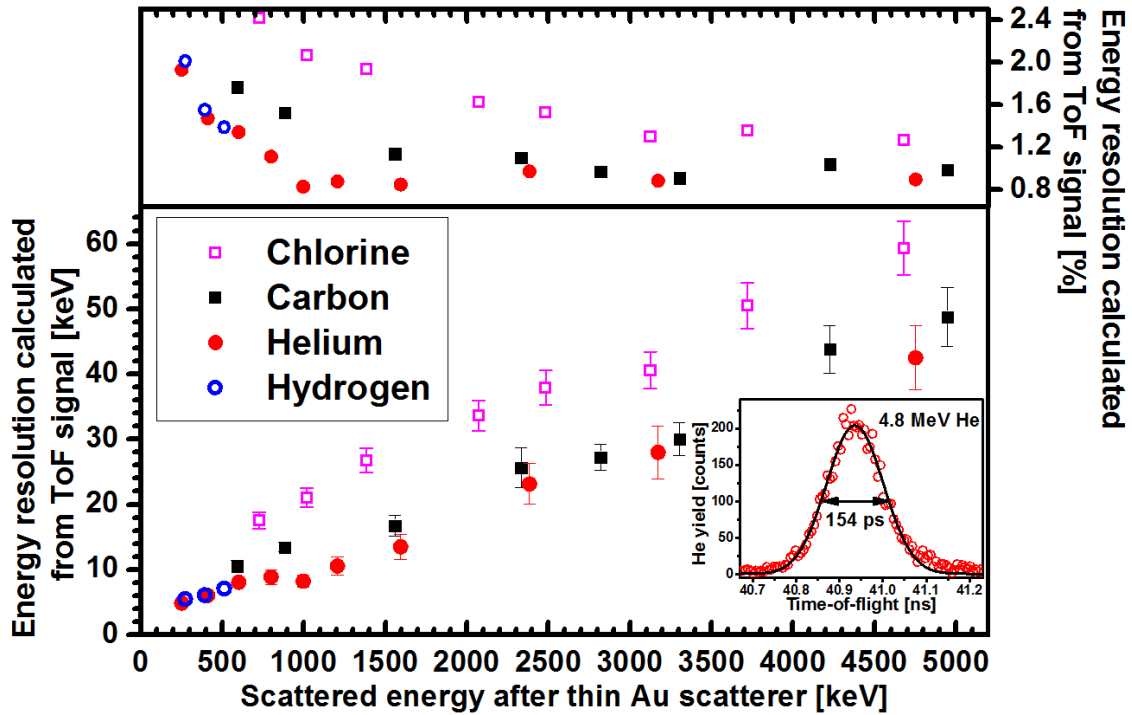
Figure 6. Energy resolution calculated from the ToF signal for different ions and energies. The measured resolution is defined as a Gaussian fit (FWHM) of the time-of-flight of the particles scattered from a thin (few Å) Au film on Si. The relative energy resolution of the time-of-flight detector approaches ~0.9 % for all ions at higher energies. The insert shows best recorded ToF-resolution of 154 ps, for 4.8 MeV He whereas the trend data for 4.8 MeV He has about 200 ps (40 keV) resolution. Different Au scatterer was used in the latter measurements and this is believed to explain the resolution difference.

The other factors that directly affect the timing resolution are the kinematic spread and the DAQ resolution. In the ToF-ERD measurements the energy spread caused by the spectrometer solid angle is up to 1.4 % for the recoiled ions in our system. The kinematic spread is close to order of magnitude lower in the case of scattered beam used in Fig. 6 results. In an average measurement with scattered 10 MeV ^{35}Cl beam, the single biggest factor degrading the timing resolution is currently induced by the TDC when using the typical 500 ns timing window. Even with 8k conversion range, the FWHM (4 ch) of the TDC alone is about 250 ps (compared to 25 ps with 50 ns timing window). However, the TDC induced spread could be diminished almost completely if fast timing digitizers would be used to directly digitize [32] the preamplified signals coming out from the timing gates.

**3.3 Data acquisition and coincidence window width**

The developed data-acquisition system uses an FPGA to retrieve the data from the TDC/ADC-unit and to time-stamp all the ToF and E events. To minimize the background, a very narrow time-interval for coincidence events should exist. Time difference of the

280 coincidence events is reduced by not using any delay line for the T1 signal but keeping
281 the T2 as the stop-detector. The time difference spread is further reduced due to the close
282 distance of the T2 foil and E-detector. Therefore events from the energy detector arrive at
283 constant time interval from the ToF-stop signal. This minimizes the time spread due to
284 the different ion velocities. The main advantage to time stamp all the events thus comes
285 from the possibility to choose the timing window width and position from the recorded
286 data, after the measurement.
287
288 The coincidence events are searched from the list-mode data after the experiment while
289 online monitoring is also build to the DAQ software. The free selection of coincidence
290 window position and width reduces the background of our measurement without losing
291 any coincident events. For typical data analysis the coincidence window width is about
292 300 ns, although majority of the events arrive within 75 ns coincidence window. The
293 minimum coincidence window width of 75 ns, 3 channels in coincident spectrum, is
294 limited by the 40 MHz clock and the TDC internal accuracy. To increase the time stamp
295 resolution the clock frequency could be doubled as noted in the manufacturer
296 specifications. The increase of the FPGA clock to 80 MHz, however, did not yield better
297 timing resolution as the data-ready signal of the TDC was not time independent at these
298 frequencies. The coincidence window width could be reduced further by using a direct
299 signal digitization with synchronized TOF and E channels. The effect of the coincidence
300 window width to the number of background events is demonstrated in the Fig. 7. From
301 the figure 7 f) one can also see that large number of hydrogen events arrive with slightly
302 different coincidence delay, in fact shorter ToF-E coincidence, compared to the majority
303 of the other ions. However, this effect for the hydrogen is mostly due to shaping amplifier
304 timing properties because of the lowest pulse amplitudes.
305
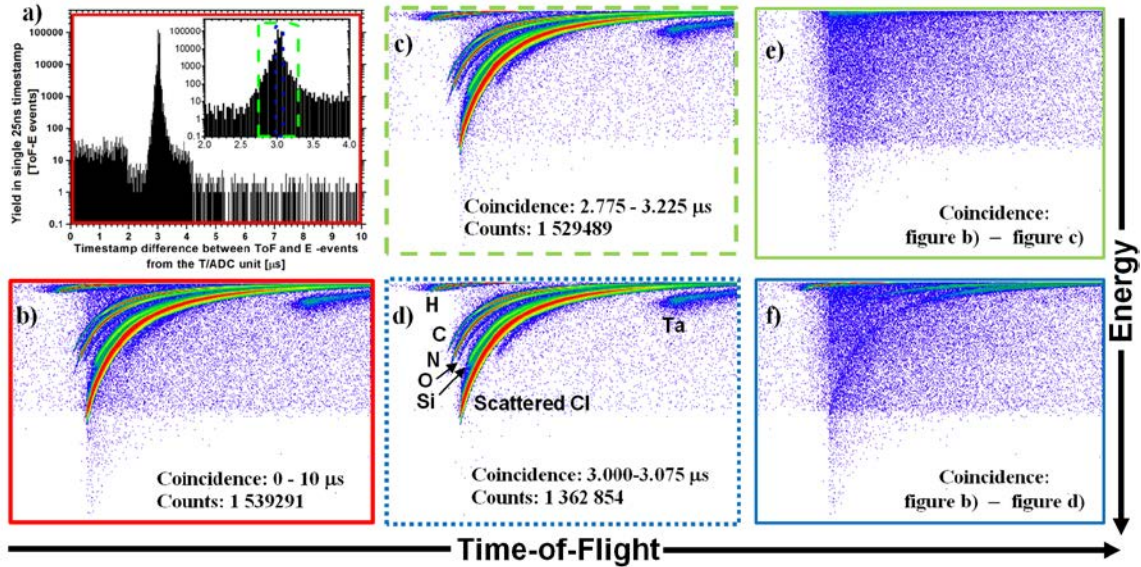
Figure 7. Effect of coincidence window width to the ToF-E background. Sample was thin TaN on Si substrate, containing lighter impurities, and sample was measured with 10 MeV $^{35}Cl^{5+}$ ions. Histogram a) shows a sharp peak at 3 μs position which indicates that most of the true ToF-E -coincidence events come with a constant time difference. All the coincidence events with shorter than 10 μs time difference are presented in b) ToF-E histogram (red rectangle). Shorter coincidence selections c) with green dashed (main ToF-E coincidence peak) and d) blue dotted (sharp, only 75 ns coincidence window) show clearly reduced number of background events. In e) and f) are shown the reduced events from the c) and d), respectively.

3.4 The different origins of the background in the ToF-energy histograms

Several types of background events normally exist in the measured data that cannot be rejected by tightening the coincidence window. Examples of these are shown in Fig. 8 which is a ToF-E histogram of 35 nm Au on Si sample measured with 6.8 MeV $^{12}C^{3+}$. Scattered beam in the insert of Fig. 8 is 10.2 MeV $^{35}Cl^{5+}$. In the Fig. 8, the recoiled Si from the substrate is also visible together with the nitrogen scattered from the Au. This nitrogen originates from the accelerator terminal stripper system. The phenomena responsible for the different backgrounds marked from **A** to **F** in the Fig. 8 are discussed below in alphabetical order and **A** to **F** always refers to the same Fig. 8.

3.4.1 Low energy tail with correct time of flight

The background marked by **A** in the Fig. 8 reduces the detection limit for the low mass elements if heavier mass exists in the same thin film. Similar low energy tails with correct ToFs can also be seen in related publications [12,13,33] by others.

When the measurement in Fig. 8 was reproduced with the same statistics but only 1/10 of the count rate, the normal pile-up **D** disappeared completely, the background **B** reduced also to about 1/10 but the background marked by **A** did not change. Compared to the main scattered peak in the Fig. 8 there exists less than 0.3 % counts in **A**. This effect is still without a definite explanation in our measurements but at least two very different causes could be reasoned for this. The easiest explanation for **A** would be some non-uniform layer between the T2 foil front surface and energy detector active area that would reduce the particle's energy before an active area in the E-detector. This would imply a) non-uniform T2 foil, b) a dust particle on the T2 foil or E detector surface c) non-uniform dead layer of the E-detector entrance window. Second phenomen that could produce a similar shape to the low energy tail is scattering that could occur for example from the rounded edges of the T2 carbon foil holder or E-detector edges depending on the distance to the T2 foil. Also large angle collisions in the T2 foil or in the energy detector can result in a similar shape.

In our case, there has been a permanent non-uniform area in the T2 carbon foil: the 20 μm thick supporting wire that is point welded to carbon foil support frame to prevent bending of the foil due to the electric field. Total area of this wire is close to 0.2 % of the solid angle, but being so thick, only the outermost edges of the wire are thin enough for heavy ions to pass the wire with only fractional energy loss. Tested removal of the wire did not cause a change in the histogram. Also, background **A** is not affected only due to the silicon detector properties only as it can also be seen in ToF-ERD histograms with gas ionization detector during our preliminary tests and in [13]. However, tests done on the ETH Zurich gas ionization chambers have shown that by changing the gas from isobutane to Ar with heavier nuclear mass the background **A** has clearly increased [34]. This would indicate that a strong candidate for the low energy background **A** could be the large angle nuclear collisions in the T2 foil or after it. To summarize the low energy tail: since different pulse height defect processes in Si detectors (high charge density, hard Si recoils, delayed charge collection, increasing radiation damage, etc.) are asymmetric, meaning more processes leading to a loss than to a gain in collected charge; this must result a tail in the spectra.

3.4.2 High count rate in at least one timing gate
In the case of **B**, the majority of the background events in both figures 6 and 8 originate from the events for which the recorded time-of-flight, associated with the E-signal, is too long. This phenomenon is generally caused by two time wise close events at T1 where DAQ does not react on the latter start, but the latter ion is the one causing the stop and E-event. Similarly, but vice versa occurring events can result in short ToFs, as would have occurred in the case of Fig. 5 where digitizer was used for T2. Despite the two collimators before the T1, free electrons and ions emitted from the sample and chamber walls during the ion bombardment increase the T1 count rate. The larger solid angle of both T1 and T2 compared to E cannot be the only explanation for the differences in the individual counting rates. These events in **B** in which more than one start or stop signal exists in a single coincidence window cannot be easily removed by analogue electronics but with digitizers programmed to inspect the whole timing window length, the removal of events with multiple starts or stops is possible.

382

383
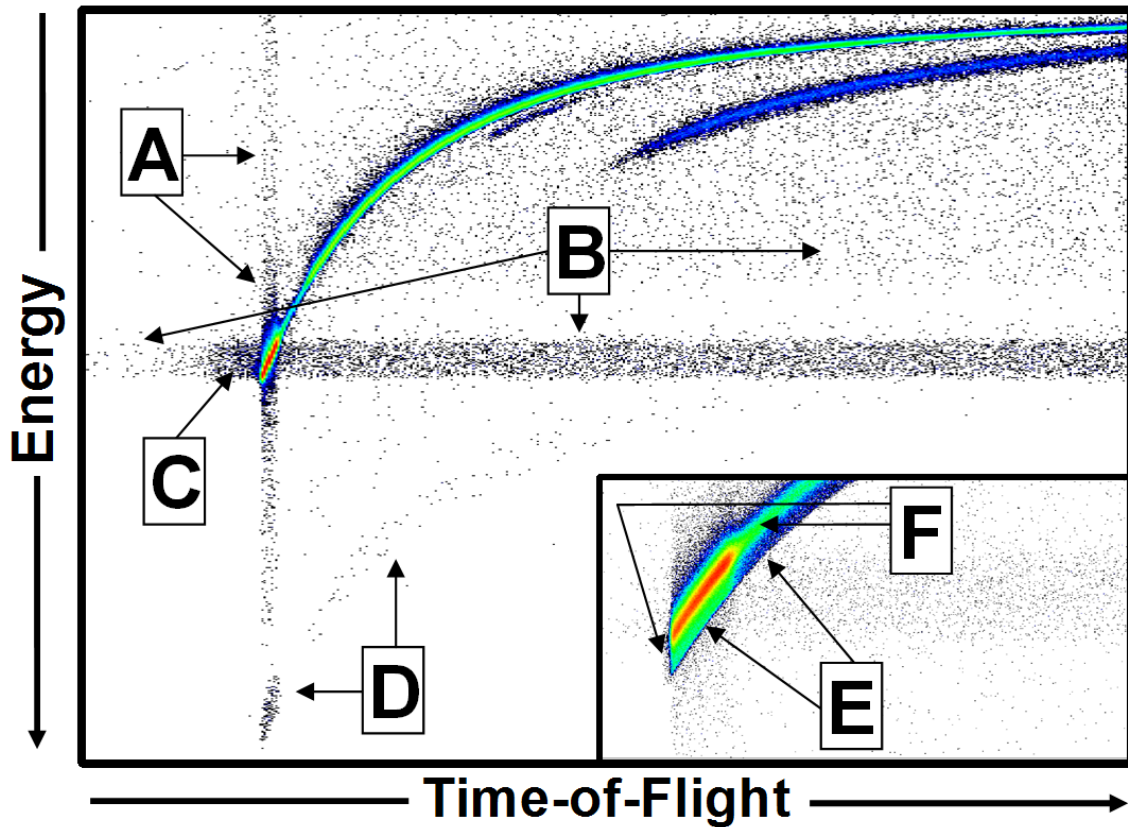
Figure 8. Demonstration of different effects that can introduce background events to the ToF-ERD measurements. Here 6.8 MeV C^{3+} probed 35 nm Au film on Si substrate. The insert shows Au peak on the same sample measured with 10.2 MeV $^{35}Cl^{5+}$. In the histogram recoils from Si substrate are also visible as well as a small amount of nitrogen, which originates from the terminal stripper system of the accelerator. Count rate was relatively high: ~4000 count/s at the energy detector, up to ~80 000 count/s at the T1 start detector and ~12 000 count/s at T2. The noise effects in the histogram are listed as follows: A: energy-detector low energy tail due to energy loss between T2-foil and E-detector, not count rate dependent. B: time-of-flight -detector's background effect due to high count rate where wrong stop/start is initiated, correlates directly to count rate. C: a halo-effect that is believed to originate from the electron scattering at MCP surface, not count rate dependent. D: energy-detector pile-up due to the high count rate. E: pulse height defect due to the channeling in the E-detector, seen as a sharp high energy edge. F: multiple scattering resulting a low energy tail and few events also at the higher energies.

3.4.3 Halo effect with correct energy for lightest ions

Far more difficult to avoid are the events that we believe is causing the additional small spread in ToF marked by **C**. This fluctuation or halo in the ToF (up to 10-20 ns) appears only for the lightest ions (no halo in Fig. 8 insert measured with ^{35}Cl) and is most pronounced for the case of hydrogen as also seen in the Fig. 9, [33] and [11] for example. For hydrogen this halo is also stronger at higher energies. This effect has been studied

405 with electron trajectory simulations by us and it can be concluded to originate after a
406 single electron emission from the carbon, and this electron is backscattered from the
407 MCP surface before entering the MCP active pore and creating a low amplitude signal.
408 This effect is examined and explained in more detail in [35].
409
410 **3.4.4 Pile-up and channeling in the energy detector and multiple scattering**
411 Count rate dependent energy pile-up marked by **D** can be removed by lowering the
412 counting rate of the energy detector or by pile-up rejection implemented in the analogue
413 electronics or by means of digitizers.
414
415 In the insert of the Fig. 8 the channeling effect **E** in a silicon energy detector is clearly
416 visible [36--38]. As the channeling effect reduces nuclear collisions in the energy
417 detector crystal the channeled ions lose more energy through electronic interactions. This
418 leads to a higher collected charge and shifts the energy signal considerably towards the
419 higher energies, especially for heavier ions. Channeling effect can be reduced by tilting
420 the silicon detector or even can be avoided by using a gas ionization chamber as an
421 energy detector.
422
423 The **F** in Fig. 8 represents multiple scattering events which often can be seen as low and
424 high energy tails in the histograms. **F** is caused by random process and therefore cannot
425 be completely avoided. Less multiple scattering takes place with light, higher energy
426 incident particles (example use of 10 MeV ^{35}Cl as an incoming ion beam compared to
427 same energy ^{63}Cu) but on the other hand the use of lighter beam introduces greater
428 elemental losses during the measurement for the same collected recoil statistics.
429
430 **3.5 Thin film analysis example**
431
432 The Jyväskylä ToF-ERD spectrometer has actively been used for measuring thin films
433 deposited by various ways. Majority of the samples have been related to the ALD
434 development like ruthenium films [39], AlN films [40], Al_2O_3/TiO_2 nanolaminates [41],
435 iridium [42], ZnO [43], silver [44], copper [45], osmium [46] and TiO_2 [47] to mention a
436 few. While thinnest quantified layers have contained only 1,2,3-5 ALD cycles of Al_2O_3
437 on TiO_2 [48], corresponding to 1-5 Å thicknesses, the thinnest actually depth profiled
438 film has been a 5 nm thick Al_2O_3 -layer on Si (see Fig. 9). Although not completely box-
439 like profile on top of the Si substrate, the flat-top region is clear on the depth profile for
440 both main components of the thin film in Fig. 9. Majority of the broadening of the
441 spectrum at the surface and interface in Fig. 9 is caused by the kinematic spread.
442
443

444
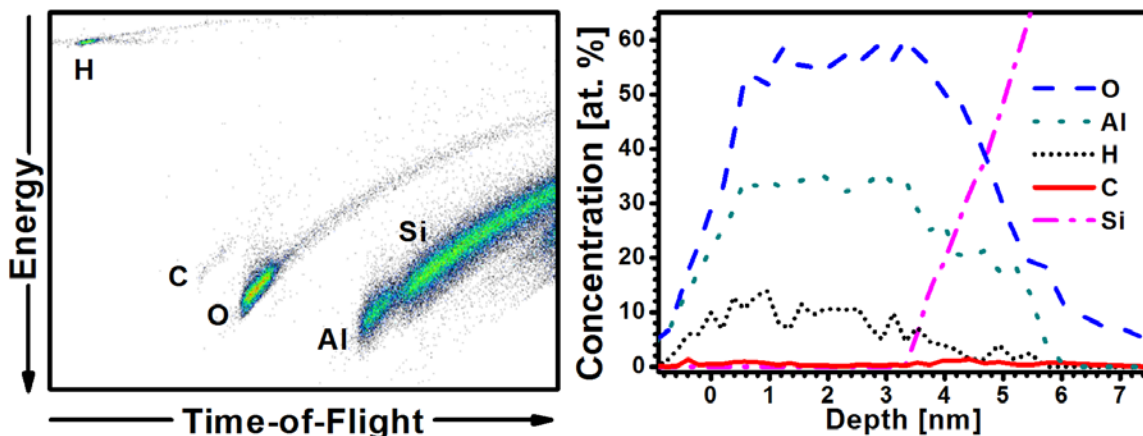
Figure 9. A raw ToF-E histogram (left) and corresponding depth profile (right) of 5 nm thick Al$_2$O$_3$ film on Si. No events are omitted from the histogram. Sample was measured with 5.1 MeV Cl^{2+} beam and the tilt angle was 2.75 degrees from the sample surface towards the detector. Density of 3.1 g/cm^3 determined by X-ray reflectivity measurements was used to convert the depth profile from at. cm^{-2} to nm. Thin film was deposited by Oili Ylivaara at VTT, Finland and XRR measurement was done by Sakari Sintonen at Aalto University, Finland.

4 Conclusions

Time-of-flight elastic recoil detection spectrometer has been built in the Jyväskylä Accelerator Laboratory. The performance of the ToF-ERD spectrometer is a sum of different properties that include design and construction of the timing detectors, detection efficiency, timing resolution and low background due to the time stamping of each event by the FPGA-based data-acquisition. ToF-detection efficiency was improved by means of coating the T1 carbon foil with thin ALD-Al$_2$O$_3$ having higher secondary electron yield than that of the graphite.

An energy resolution of 1.0 % or better for an energy calculated from the ToF signal was achieved for the ion beam scattered from a thin Au target. In our system, however, the detector solid angle can introduce a maximum spread of 1.4 % to the recoil energy, and this cannot be avoided without a kinematic correction. The TDC system with 500 ns timing window width limits currently the ToF resolution as much as the kinematic spread. This TDC induced limitation, however, can be diminished in the future by using fast digitizers for direct signal digitization. Improvement to the ToF resolution could also be achieved by reducing straggling in the T1 by using thin DLC foils, which would most likely need to be coated in order to enhance the secondary electron emission.

For the high count rates a large contribution to the background comes from the events where two start signals are generated at T1 but only the latter event will generate the stop and E signal. This type of background can at least be partly removed by fast signal digitizers, and tight coincidence window can already reduce the background significantly.

Achieved timing resolution of the ToF-ERD spectrometer has enabled us to regularly depth profile thinner than 10 nm thick films. To improve the energy detection resolution and mass resolution for heavy elements, the solid state silicon detector has to be changed to the gas ionization chamber with thin Si_3N_4 window, which is currently under development.

Acknowledgements

References:

[1] H.J. Whitlow, G. Possnert, C.S. Petersson, Nucl. Instr. and Meth. B, 27 (1987), p. 448.

[2] J. Thomas, M. Fallavier, A. Ziani, Nucl. Instr. and Meth. B, 15 (1986), p. 443.

[3] R. Groleau, S. Gujrathi, J. Martin, Nucl. Instr. and Meth., 218 (1983), p. 11.

[4] J.F. Ziegler and J.P. Biersack, Treatise on Heavy-Ion Science, (1985), p. 93.

[5] J. F. Ziegler, SRIM-2008.04, www.srim.org, 2008.

[6] R. Betts, Nucl. Instr. and Meth., 162 (1979), p. 531.

[7] M. Döbeli, C. Kottler, M. Stocker, S. Weinmann, H. Synal, M. Grajcar, M. Suter, Nucl. Instr. and Meth. B, 219 (2004), p. 415.

[8] C. Kottler, M. Döbeli, F. Glaus, M. Suter, Nucl. Instr. and Meth. B, 248 (2006), p. 155.

[9] F. Busch, W. Pfeffer, B. Kohlmeyer, D. Schüll, F. Pühlhoffer, Nucl. Instr. and Meth., 171 (1980), p. 71.

[10] M. Döbeli, C. Kottler, F. Glaus, M. Suter, Nucl. Instr. and Meth. B, 241 (2005), p. 428.

[11] S. Giangrandi, T. Sajavaara, B. Brijs, K. Arstila, A. Vantomme, W. Vandervorst, Nucl. Instr. and Meth. B, 266 (2008), p. 5144.

511   [12] Z. Siketić, I.B. Radović, M. Jakšić, Nucl. Instr. and Meth. B, 266 (2008), p. 1328.

512   [13] C. Kottler, *Dünnschichtanalyse mittels Vorwärtsstreuung bei tiefer Energie* (ETH
513   Zürich, 2005) PhD. thesis.

514   [14] M. Döbeli, R. Ender, V. Liechtenstein, D. Vetterli, Nucl. Instr. and Meth. B, 142
515   (1998), p. 417.

516   [15] Tectra, *Microchannel Plates and Microchannel Plate Detectors*,
517   http://www.tectra.de/MCP.htm (25.2.1013).

518   [16] Hamamatsu Photonics, *MCP assembly, technical information - datasheet (2006)*.

519   [17] R. Goruganthu and W. Wilson, Rev. Sci. Instrum., 55 (1984), p. 2030.

520   [18] M. Galanti, R. Gott, J. Renaud, Rev. Sci. Instrum., 42 (1971), p. 1818.

521   [19] ACF-METALS, *Thin carbon foils*, http://www.techexpo.com/firms/acf-metl.html
522   (8.3.2013).

523   [20] Luma-metal, *Gold Plated Tungsten Wire*, http://www.luma-metall.se/products/gold-
524   plated-tungsten-wire (25.2.2013).

525   [21] Canberra, *Passivated Implanted Planar Silicon (PIPS) detector*,
526   http://www.canberra.com/products/detectors/pips-detectors.asp (8.3.2013).

527   [22] Julin J. et al., To be published later in Nucl. Instr. and Meth. B, (2013/2014).

528   [23] National Instruments, *PXI-7811R-FPGA product pages*,
529   http://sine.ni.com/nips/cds/view/p/lang/en/nid/13862 (2012).

530   [24] R.A. Baragiola, Nucl. Instr. and Meth. B, 78 (1993), p. 223.

531   [25] E. Sternglass, Phys. Rev., 108 (1957), p. 1.

532   [26] Y. Zhang, H.J. Whitlow, T. Winzell, I.F. Bubb, T. Sajavaara, K. Arstila, J.
533   Keinonen, Nucl. Instr. and Meth. B, 149 (1999), p. 477.

534   [27] C.G. Drexler and R.D. DuBois, Phys. Rev. A, 53 (1996), p. 1630.

535   [28] W. Bohne, J. Röhrich, G. Röschert, Nucl. Instr. and Meth. B, 136 (1998), p. 633.

536   [29] R.L. Puurunen, J. Appl. Phys., 97 (2005), p. 121301.

537   [30] K. McDonald, R.A. Weller, V.K. Liechtenstein, Nucl. Instr. and Meth. B, 152
538   (1999), p. 171.

539 [31] V.K. Liechtenstein, T. Ivkova, E. Olshanski, I. Feigenbaum, R. DiNardo, M. Döbeli,
540 Nucl. Instr. and Meth. A, 397 (1997), p. 140.

541 [32] L. Bardelli, G. Poggi, M. Bini, G. Pasquali, N. Taccetti, Nucl. Instr. and Meth. A,
542 521 (2004), p. 480.

543 [33] S. Giangrandi, *Low-energy Elastic Recoil Detection and Ion Beam Analysis for*
544 *quantitative elemental profiling of thin films* (KU Leuven, 2010) PhD. thesis.

545 [34] Max Döbeli, Private discussion, (10.9.2013).

546 [35] Laitinen M. et al., To be published later in Nucl. Instr. and Meth. A, (2013).

547 [36] W. Pilz, J. Borany, R. Grötzschel, W. Jiang, M. Posselt, B. Schmidt, Nucl. Instr. and
548 Meth. B, 419 (1998), p. 137.

549 [37] A. Grob, J. Grob, P. Siffert, Nucl. Instr. and Meth., 132 (1976), p. 273.

550 [38] W. Sullivan and B. Wehring, Nucl. Instr. and Meth., 116 (1974), p. 29.

551 [39] K. Kukli, M. Kemell, E. Puukilainen, J. Aarik, A. Aidla, T. Sajavaara, M. Laitinen,
552 M. Tallarida, J. Sundqvist, M. Ritala, M. Leskelä, J. Electrochem. Soc., 158 (2011), p.
553 D158.

554 [40] M. Bosund, T. Sajavaara, M. Laitinen, T. Huhtio, M. Putkonen, V. Airaksinen, H.
555 Lipsanen, Appl. Surf. Sci., 257 (2011), p. 7827.

556 [41] M. Laitinen, T. Sajavaara, M. Rossi, J. Julin, R.L. Puurunen, T. Suni, T. Ishida, H.
557 Fujita, K. Arstila, B. Brijs, Whitlow H.J, Nucl. Instr. and Meth. B, 269 (2011), p. 3021.

558 [42] J. Hämäläinen, T. Hatanpää, E. Puukilainen, T. Sajavaara, M. Ritala, M. Leskelä, J.
559 Mater. Chem., 21 (2011), p. 16488.

560 [43] J. Malm, E. Sahramo, J. Perälä, T. Sajavaara, M. Karppinen, Thin Solid Films, 519
561 (2011), p. 5319.

562 [44] M. Kariniemi, J. Niinistö, T. Hatanpää, M. Kemell, T. Sajavaara, M. Ritala, M.
563 Leskelä, Chem. Mater., 23 (2011), p. 2901.

564 [45] T.J. Knisley, T.C. Ariyasena, T. Sajavaara, M.J. Saly, C.H. Winter, Chem. Mater.,
565 23 (2011), p. 4417.

566 [46] J. Hämäläinen, T. Sajavaara, E. Puukilainen, M. Ritala, M. Leskelä, Chem. Mater.,
567 24 (2011), p. 55.

568   [47] R.L. Puurunen, T. Sajavaara, E. Santala, V. Miikkulainen, T. Saukkonen, M.
569   Laitinen, M. Leskela, J. Nanosci. Technol., 11 (2011), p. 8101.

570   [48] L.J. Antila, M. J. Heikkilä, V. Mäkinen, N. Humalamäki, M. Laitinen, V. Linko, P.
571   Jalkanen, J. Toppari, V. Aumanen, M. Kemell, P. Myllyperkiö, K. Honkala, H.
572   Häkkinen, M. Leskelä, J.E.I. Korppi-Tommola, J. Phys. Chem. C, 115 (2011), p. 16720.

573